Walker, K. Wieghardt, and K. Yamanouchi. Special thanks are expressed to Dr. Parkin for preprints of refs 11 and 41b and to Prof. M. Hall for a preprint of ref 10b. This work was supported in part by the National Institutes of Health (Grants GM37773 to J.H.E. and GM18865 to T.M.L.), the Materials Characterization Program of the University of Arizona, and the North Atlantic Treaty Organization (Grant 86/0513).

Registry No. $MoOCl_2(PMe_2Ph)_3$, 30134-06-6; $MoCl_3(PMe,Ph)_3$, 36926-67-7.

A Highly Reactive Functional Model for the Catechol Dioxygenases. Structure and Properties of [Fe(TPA)DBC]BPh_4

Ho G. Jang, David D. Cox, and Lawrence Que, Jr.*

Contribution from the Department of Chemistry, University of Minnesota, Minneapolis, Minnesota 55455. *Received May 2, 1991*

Abstract: [Fe^{III}(TPA)DBC]BPh_4, a new functional model for the catechol dioxygenases, has been synthesized, where TPA is tris(2-pyridylmethyl)amine and DBC is 3,5-di-*tert*-butylcatecholate dianion. The TPA complex reacts with O_2 within minutes to afford intradiol cleavage, in 98% yield, which is the highest conversion observed of all [Fe(L)DBC] complexes studied. More interestingly, the TPA complex is the fastest reacting of all the [Fe(L)DBC] complexes studied. Kinetic studies of the reaction of the complex with 1 atm of O_2 in DMF under pseudo-first-order conditions show that the TPA complex reacts approximately three orders of magnitude faster than the corresponding NTA complex, where NTA is *N*,*N*-bis(carboxymethyl)glycine. Both the high specificity and the fast kinetics can be associated with the high Lewis acidity of the ferric center in the TPA complex. To investigate the factors determining reactivity, we have solved the crystal structure of [Fe(TPA)DBC]BPh_4 (space group $P\bar{1}$, a = 12.464 (5) Å, b = 13.480 (6) Å, c = 15.980 (8) Å, α = 85.11 (4)°, β = 83.96 (4)°, γ = 70.76 (4)°, V = 2517 (4) Å^3, Z = 2, R = 0.054 and R_w = 0.063). Compared with other complexes in the [Fe(L)DBC] series, the iron-catecholate interaction in the TPA complex is significantly stronger, resulting in the enhanced covalency of the metal-catecholate bonds and low-energy catecholate LMCT bands. The enhanced covalency is reflected by the isotropic shifts exhibited by the DBC protons, which indicate increased semiquinone character. The greater semiquinone character in the TPA complex correlates well with its high reactivity toward O_2. These trends provide substantial evidence for the substrate activation mechanism proposed for the oxidative cleavage of catechols.

The catechol dioxygenases catalyze the oxidative cleavage of catechols and serve as part of nature's strategy for degrading aromatic molecules in the biosphere.[1] Significant progress[2-7] has been made in understanding the active site of the intradiol cleaving enzymes and is highlighted by the recent solution of the crystal structure of native protocatechuate 3,4-dioxygenase.[8] Functional mimics for these enzymes have also been developed since the flexibility in ligand design allows a systematic study of the important factors affecting reactivity as well as reaction mechanism.[9-12] In our biomimetic efforts, we have focused on obtaining structurally characterized complexes capable of oxidative cleavage activity.[10,12] By studying a series of [Fe^{III}(L)DBC][13] complexes

Scheme I

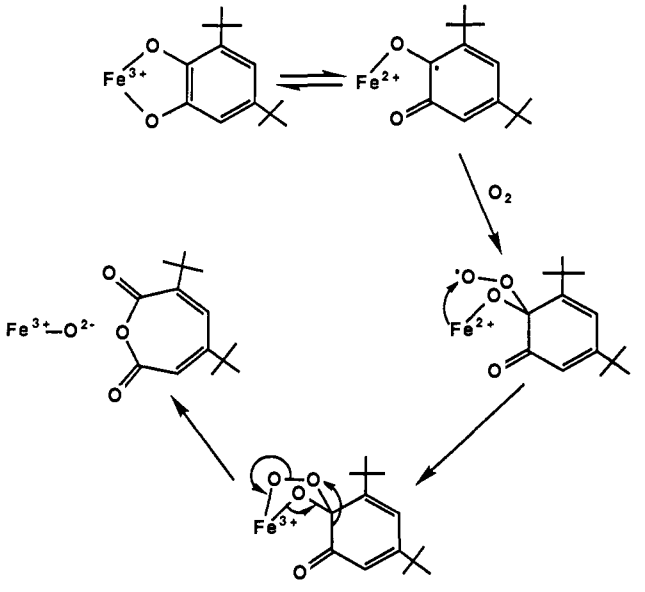

where L is a tetradentate tripodal ligand, we have demonstrated a direct correlation between the rate of oxidative cleavage of the bound catecholate ligand and the Lewis acidity of the ferric center,

(1) For recent reviews of these enzymes, see: Que, L., Jr. *Adv. Inorg. Biochem.* **1983**, *5*, 167. Que, L., Jr. *J. Chem. Educ.* **1985**, *62*, 938. Que, L., Jr. In *Iron Carriers and Iron Proteins*; Loehr, T. M., Ed.; VCH Publishers: New York, 1989; p 467.

(2) (a) Whittaker, J. W.; Lipscomb, J. D.; Kent, T. A.; Münck, E. *J. Biol. Chem.* **1984**, *259*, 4466. (b) Kent, T. A.; Münck, E.; Pyrz, J. W.; Widom, J.; Que, L., Jr. *Inorg. Chem.* **1987**, *26*, 1402.

(3) (a) Que, L., Jr.; Heistand, R. H., II; Mayer, R.; Roe, A. L. *Biochemistry* **1980**, *19*, 2588. (b) Que, L., Jr.; Epstein, R. M. *Biochemistry* **1981**, *20*, 2545.

(4) Whittaker, J. W.; Lipscomb, J. D. *J. Biol. Chem.* **1984**, *259*, 4487.

(5) (a) Felton, R. H.; Barrow, W. L.; May, S. W.; Sowell, A. L.; Goel, S. *J. Am. Chem. Soc.* **1982**, *104*, 6132. (b) True, A. E.; Orville, A. M.; Pearce, L. L.; Lipscomb, J. D.; Que, L., Jr. *Biochemistry*, **1990**, *29*, 10847.

(6) Que, L., Jr.; Lauffer, R. B.; Lynch, J. B.; Murch, B. P.; Pyrz, J. W. *J. Am. Chem. Soc.* **1987**, *109*, 5381.

(7) (a) Bull, C.; Ballou, D. P.; Otsuka, S. *J. Biol. Chem.* **1981**, *256*, 12681. (b) Walsh, T. A.; Ballou, D. P.; Mayer, R.; Que, L., Jr. *J. Biol. Chem.* **1983**, *258*, 14422.

(8) Ohlendorf, D. H.; Lipscomb, J. D.; Weber, P. C. *Nature* **1988**, *336*, 403.

(9) (a) Funabiki, T.; Tada, S.; Yoshioka, T.; Takano, M.; Yoshida, S. *J. Chem. Soc., Chem. Commun.* **1986**, 1699. (b) Funabiki, T.; Mizoguchi, A.; Sugimoto, T.; Tada, S.; Tsuji, M.; Yoshioka, T.; Sakamoto, H.; Takano, M.; Yoshida, S. *J. Am. Chem. Soc.* **1986**, 108, 2921. (c) Funabiki, T.; Konishi, T.; Kobayashi, S.; Mizoguchi, A.; T. M.; Takano, M.; Yoshida, S. *Chem. Lett.* **1987**, 719.

(10) Que, L., Jr.; Kolanczyk, R. C.; White, L. S. *J. Am. Chem. Soc.* **1987**, *109*, 5373.

(11) Cox, D. D.; Benkovic, S. J.; Bloom, L. M.; Bradley, F. C.; Nelson, M. J.; Que, L., Jr.; Wallick, D. E. *J. Am. Chem. Soc.* **1988**, *110*, 2026.

(12) Cox, D. D.; Que, L., Jr. *J. Am. Chem. Soc.* **1988**, *110*, 8085.

(13) Abbreviations: NTA, *N*,*N*-bis(carboxylmethyl)glycine; PDA, *N*-(carboxymethyl)-*N*-(2-pyridylmethyl)glycine; BPG, *N*,*N*-bis(2-pyridylmethyl)glycine; TPA, tris(2-pyridylmethyl)amine; $DBCH_2$, 3,5-di-*tert*-butylcatechol; py, pyridine.

0002-7863/91/1513-9200$02.50/0 © 1991 American Chemical Society

the rate-determining step involving the attack of dioxygen on the complex.[10,12] We have proposed that the increased Lewis acidity of the ferric center enhances the covalency of the metal–catecholate interaction and the semiquinone character of the bound catecholate, thereby activating the catecholate for reaction with O_2.[12] These observations provide the underlying rationale for the novel substrate activation mechanism we proposed previously.[14] In this mechanism (Scheme I), the substrate catecholate becomes activated upon coordination to the iron due to ligand-to-metal charge transfer and reacts with oxygen to yield a peroxide intermediate. This intermediate then decomposes to organic products. In this paper, we report the crystal structure and spectroscopic properties of [Fe(TPA)DBC]BPh$_4$, thus far the most reactive complex of this series, which further strengthen our arguments for the role of the metal center in the substrate activation mechanism proposed for the dioxygenases.

Experimental Section

All reagents and solvents were purchased from commercial sources and used as received, unless noted otherwise. Acetonitrile was distilled from CaH_2 under nitrogen before use. $DBCH_2$ was purified by recrystallization from hexane. $DBCH_2$-*4,6-d*$_2$ was prepared by deuterium exchange in D_2O in the presence of a substoichiometric amount of base at 140 °C in a sealed tube for ~4 h.[15] The ligand, TPA·3HClO$_4$ was synthesized according to published procedures.[16] Microanalyses were performed by M-H-W Laboratories, Phoenix, AZ.

Synthesis of Complexes. [Fe(TPA)DBC](BPh$_4$) was synthesized by reacting 153.5 mg (0.38 mmol) of Fe(NO$_3$)$_3$·9H$_2$O and 225 mg (0.38 mmol) of TPA·3HClO$_4$ in 25 mL of ethanol under argon and adding 84.5 mg (0.38 mmol) $DBCH_2$ in 3 mL of ethanol under argon after 30 min, followed by the slow addition of 6 equiv of piperidine. The resulting dark purple blue solution was treated with 130 mg (0.38 mmol) of NaBPh$_4$, causing the immediate precipitation of a purple blue powder, which was washed with ethanol and dried under vacuum (73% yield). X-ray diffraction quality crystals were obtained by vapor diffusion of ether into an acetonitrile solution of crude product. Anal. Calcd for [Fe(TPA)DBC](BPh$_4$)·(CH$_3$CN), $C_{58}H_{61}BFeN_5O_2$: C, 75.16; H, 6.63; N, 7.56. Found: C, 75.26; H, 6.75; N, 7.51.

[Fe$_2$(TPA)$_2$O(C$_{14}$H$_{21}$O$_4$)](ClO$_4$)$_3$ was synthesized following published procedures for other (μ-oxo)(μ-carboxylato)diiron(III) complexes.[17] TPA·3HClO$_4$ (118.4 mg, 0.2 mmol) and triethylamine (0.126 mL, 0.9 mmol) in 10 mL of methanol was reacted with Fe(ClO$_4$)$_3$·10H$_2$O (107.4 mg, 0.2 mmol) dissolved in 2 mL of methanol. To this mixture was added a methanol solution of 3,5-di-*tert*-butyl-5-(carboxymethyl)-2-furanone (25.4 mg, 0.10 mmol). When this mixture was allowed to stand for a few hours, microcrystals of the desired complex were obtained. UV–vis (CH$_3$CN) λ_{max}, 330, 462, 492, 710 nm; ^{1}H NMR (CD$_3$CN) δ 39, 32, 24, 22 (py ortho H or CH$_2$), 18.3, 17.3, 13.5, 13.1, 11.9 (py meta H), 8.6, 7.5, 7.0, 5.4 (py para H), and 14.3 (O_2C-CH_2-R) ppm. Anal. Calcd for [Fe$_2$(TPA)$_2$O(C$_{14}$H$_{21}$O$_4$)](ClO$_4$)$_3$, $C_{50}H_{57}Cl_3Fe_2N_8O_{17}$: C, 47.66; H, 4.60; N, 8.89. Found: C, 47.46; H, 4.80; N, 8.90.

Characterization of Oxygenation Products. The two major organic products of the [Fe(TPA)DBC]$^+$ oxygenation reaction were identified by using GC, HPLC, IR, and NMR spectroscopy. Spectroscopic data are as follows: 3,5-di-*tert*-butyl-5-(carboxymethyl)-2-furanone, IR(KBr) ν_{CO} 1755, 1723 cm^{-1}, $\nu_{C=C}$ 1644 cm^{-1}; ^{1}H NMR (CDCl$_3$) δ 0.96 (s, 9 H), 1.21 (s, 9 H), [2.74, 2.81, 2.91, 2.98 (AB q, J_{AB} = 14 Hz, 2 H)], 6.93 (s, 1 H), 9.70 (s); ^{13}C NMR (CDCl$_3$) δ 24.9 (q), 27.6 (q), 31.2 (s), 37.1 (t), 37.4 (s), 87.8 (s), 143.6 (s), 145.2 (d), 170.9 (s), 174.7 (s); 3,5-di-*tert*-butyl-1-oxacyclohepta-3,5-diene-2,7-dione, IR (KBr) ν_{CO} 1783, 1741 cm^{-1}, $\nu_{C=C}$ 1636, 1600 cm^{-1}; ^{1}H NMR (CDCl$_3$) δ 1.16 (s, 9 H), 1.28 (s, 9 H), 6.14 (d, J = 2 Hz, 1 H), 6.45 (d, J = 2 Hz, 1 H); ^{13}C NMR (CDCl$_3$) δ 28.4 (q), 28.9 (q), 36.2 (s), 36.5 (s), 115.5 (d), 123.9 (d), 148.0 (s), 160.0 (s), 162 (s).

Crystallographic Studies. A dark blue crystal of [Fe(TPA)DBC](BPh$_4$)·CH$_3$CN (dimensions: 0.70 × 0.60 × 0.45 mm) was mounted on the end of a glass fiber with a viscous high-molecular-weight hydrocarbon. Intensity data were collected at the Crystallography Facility of the University of Minnesota Chemistry Department on an Enraf-Nonius CAD4 diffractometer. Absorption corrections were made, and no signal decay was observed. The cell dimensions were obtained by least-squares refinements of the setting angles for 25 centered reflections (2θ = 28–42.4°). The structure was solved by using direct methods, and

Table I. Crystallographic Data[a] for [Fe(TPA)DBC]BPh$_4$·CH$_3$CN

formula	$C_{58}H_{58}BFeN_5O_2$
formula wt, amu	923.79
temp, K	172
crystal system	triclinic
space group	$P\bar{1}$
a, Å	12.464 (5)
b, Å	13.480 (6)
c, Å	15.980 (8)
α, deg	85.11 (4)
β, deg	83.96 (4)
γ, deg	70.76 (4)
V, Å^3	2517 (4)
Z	2
ρ(calc), g cm^{-3}	1.219
radiation	Mo Kα (λ = 0.7107 Å)
$\mu_{(MoK\alpha)}$, cm^{-1}	3.43
scan type	ω
$2\theta_{max}$, deg	51.8
indices collected	$+h,\pm k,\pm l$
no. of reflcns	9053
	6350 used ($I > 2\sigma(I)$)
no. of least sq params	757
R^b	0.054
$R_w{}^b$	0.062

[a] The intensity data were processed as described in: *CAD 4* and *SDP-PLUS User's Manual*; B. A. Frenz & Assoc.; College Station, TX, 1982. The net intensity $I = [K(NPI)](C - 2B)$, where K = 20.1166 (attenuator factor), NPI = ratio of fastest possible scan rate to scan rate for the measurement, C = total count, and B = total background count. The standard deviation in the net intensity is given by $[\sigma(I)]^2 = (k/NPI)^2[C + 4B + (pI)^2]$ where p is a factor used to downweight intense reflections. The observed structure factor amplitude F_o is given by $F_o = (I/Lp)^{1/2}$, where Lp = Lorentz and polarization factors. The $\sigma(I)$'s were converted to the estimated errors in the relative structure factors $\sigma(F_o)$ by $\sigma(F_o) = {}^1/_2[\sigma(I)/I]F_o$. [b] $R = (\sum||F_o| - |F_c||)/(\sum F_o)$; $R_w = [(\sum w|F_o - F_c|^2)/(\sum w(F_o)^2)]^{1/2}$.

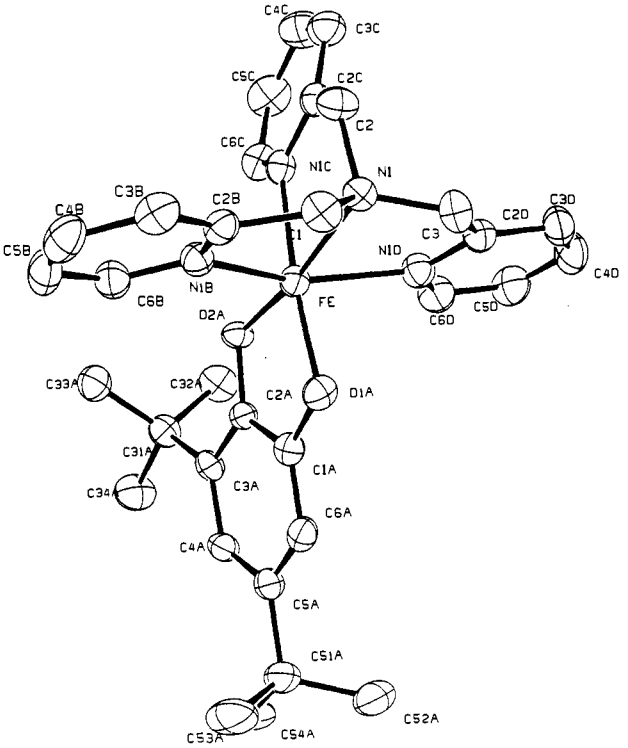

Figure 1. Structure of the [Fe(TPA)DBC]$^+$ in the crystal of **1** showing the 50% probability thermal ellipsoids and atom labeling scheme. Hydrogen atoms omitted for clarity

(14) Que, L., Jr.; Lipscomb, J. D.; Münck, E.; Wood, J. M. *Biochim. Biophys. Acta* **1977**, *485*, 60.
(15) Pyrz, J. W.; Roe, A. L.; Stern, L. J.; Que, L., Jr. *J. Am. Chem. Soc.* **1985**, *107*, 614.
(16) Gafford, B. G.; Holwerda, R. A. *Inorg. Chem.* **1989**, *28*, 60.
(17) (a) Norman, R. E.; Yan, S.; Que, L., Jr.; Backes, G.; Ling, J.; Sander-Loehr, J.; Zhang, J. H.; O'Connor, C. J. *J. Am. Chem. Soc.* **1990**, *112*, 1554. (b) Norman, R. E.; Holz, R. C.; Menage, S.; O'Connor, C. J.; Zhang, J. H.; Que, L.; Jr. *Inorg. Chem.* **1990**, *29*, 4629.

Table II. Selected Bond Lengths (Å) and Angles (deg) for [Fe(TPA)DBC]BPh_4·CH_3CN[a]

Bond Lengths (Å)			
Fe–O1A	1.917 (3)	C3–C2D	1.505 (5)
Fe–O2A	1.898 (2)	N1B–C2B	1.355 (4)
Fe–N1	2.221 (3)	C2B–C3B	1.372 (5)
Fe–N1B	2.105 (3)	C3B–C4B	1.379 (5)
Fe–N1C	2.145 (3)	C4B–C5B	1.377 (5)
Fe–N1D	2.142 (3)	C5B–C6B	1.369 (5)
C1A–O1A	1.347 (4)	C6B–N1B	1.341 (4)
C2A–O2A	1.349 (4)	N1C–C2C	1.346 (4)
C1A–C2A	1.418 (5)	C2C–C3C	1.376 (5)
C2A–C3A	1.405 (4)	C3C–C4C	1.380 (6)
C3A–C4A	1.403 (5)	C4C–C5C	1.373 (5)
C4A–C5A	1.395 (5)	C5C–C6C	1.373 (5)
C5A–C6A	1.390 (5)	C6C–N1C	1.345 (4)
C6A–C1A	1.382 (5)	N1D–C2D	1.347 (4)
N1–C1	1.482 (4)	C2D–C3D	1.374 (5)
N1–C2	1.487 (4)	C3D–C4D	1.382 (5)
N1–C3	1.475 (4)	C4D–C5D	1.367 (6)
C1–C2B	1.491 (5)	C5D–C6D	1.377 (5)
C2–C2C	1.511 (5)	C6D–N1D	1.347 (5)
Bond Angles (deg)			
N1–Fe–N1B	76.2 (1)	O2A–Fe–N1D	104.0 (1)
N1–Fe–N1C	79.9 (1)	N1B–Fe–N1C	96.5 (1)
N1–Fe–N1D	76.8 (1)	N1B–Fe–N1D	152.8 (1)
N1–Fe–O1A	103.5 (1)	N1C–Fe–N1D	82.0 (1)
N1–Fe–O2A	171.3 (1)	Fe–N1–C1	106.4 (2)
O1A–Fe–N1B	92.3 (1)	Fe–N1–C2	107.8 (2)
O1A–Fe–N1C	171.1 (1)	Fe–N1–C3	108.1 (2)
O1A–Fe–N1D	90.7 (1)	Fe–O1A–C1A	111.4 (2)
O1A–Fe–O2A	85.2 (1)	Fe–O2A–C2A	112.2 (2)
O2A–Fe–N1B	103.2 (1)	O1A–C1A–C2A	115.7 (3)
O2A–Fe–N1C	91.6 (1)	O2A–C2A–C1A	123.9 (3)

[a] Estimated standard deviations in the least significant digits are given in parentheses.

crystallographic and refinement data are summarized in Table I. All non-H atoms were refined with anisotropic thermal parameters. Hydrogen atoms were included in the structure factor correlation in idealized positions (d(C–H) = 0.95 Å, B_H = 3.0). The standard deviation of an observation of unit weight was 1.44. The weighting scheme was based on counting statistics and included a factor (p = 0.05) to downweight the intense reflections. The maximum and minimum peaks on the final difference Fourier map corresponded to 0.45 and −0.53 $e^-/Å^3$, respectively. Neutral atom scattering factors (including anomalous scattering) were used.[18] All calculations were performed by using TEXSAN Crystallographic shoftware package of the Molecular Structure Corp. An ORTEP plot of the structure of the cation is shown in Figure 1, together with the numbering scheme for the complex. Selected bond lengths and bond angles are listed in Table II, while atomic coordinates, thermal parameters, and a complete listing of bond lengths and angles are available as supplementary material.

Physical Methods. UV–visible spectra were obtained on a Hewlett-Packard 8451 diode array spectrophotometer. The near-IR spectrum was recorded with a Cary 14 spectrometer interfaced to a OLIS computer system. IR spectra were obtained with a Perkin-Elmer 1710 FT-IR spectrometer. Standard organic product analyses were performed using a Perkin-Elmer Sigma 3 gas chromatograph equipped with a flame ionization detector or a reverse-phase isocractic HPLC (Waters 6000A isocractic system; Kratos 769Z variable wavelength detector, 240 nm; Whatman Partisil ODS-5 C18 column). ^1H NMR spectra were obtained on an IBM AC300 spectrometer. ^2H NMR spectra were obtained on a Varian VXR300 spectrometer. An inversion-recovery pulse sequence (180°–τ–90°–ACQ) was used to obtain nonselective proton longitudinal relaxation times (T_1) with carrier frequency set at several different positions to ensure the validity of the measurements.

Oxygenation Studies. Reactivity studies were performed in organic solvents in an oxygen atmosphere under ambient conditions. After the reaction was complete, as indicated by the loss of color, the solution was concentrated under reduced pressure. The anhydride product was extracted with ether, dried over anhydrous Na_2SO_4, and then concentrated. The remaining residue was dissolved in DMF or CH_3CN and acidified with HCl to pH 3 to decompose the dinuclear Fe^{III}TPA complex. The furanone acid was extracted with ether, dried, and concentrated. The extracts were then subjected to GC or reverse-phase isocractic HPLC separation (conditions are the same as previously reported in ref 12).

Kinetic studies were performed on an HP-8451 diode array spectrometer with temperature control by an Endocal RTE-5 refrigerated circulation bath. Oxygen was bubbled through the solution (0.5–0.8 mM in complex) and then maintained at 1 atm of pressure above the reacting solution. The oxygenation kinetics were followed by monitoring the disappearance of the low-energy charge-transfer band of the TPA complex.

Results and Discussion

[Fe(TPA)DBC]BPh_4 is an air-sensitive purple blue solid derived from the stoichiometric combination of its three components in the presence of base, followed by metathesis with $NaBPh_4$. The complex exhibits two catecholate-to-Fe(III) charge-transfer bands at 568 and 883 nm (ϵ = 1460 and 1800 M^{-1} cm^{-1}, respectively), which have intensities (ϵ = 1200–2500 M^{-1} cm^{-1}) similar to those of previous [Fe(L)DBC] complexes.[11] However, these values are the most red-shifted of the [Fe(L)DBC] series (Table III). The low energies of these transitions clearly demonstrate the large Lewis acidity of the Fe(III) center in the TPA complex, which is not surprising since TPA is the only tripodal ligand in the series to provide all neutral nitrogen ligands. The spectral characteristics of this complex are similar to those reported by Funabiki for the complex of $FeCl_3$ and $DBCH_2$ in pyridine which affords some intradiol cleavage product upon exposure to air.[9] This latter species is not well-characterized, but its similarities to [Fe(TPA)-DBC]BPh_4 implicates an analogous ligand environment, perhaps consisting of $[Fe(py)_4DBC]^+$.

Crystal Structure of [Fe(TPA)DBC](BPh_4)·CH_3CN. To complete our structural studies of the [Fe(L)DBC] series, we have crystallized [Fe(TPA)DBC]BPh_4 and solved its structure (Table I and Figure 1). Like previously characterized members of this series, $[Fe(NTA)DBC]^{2-}$ [10] and [Fe(BPG)DBC],[12] [Fe(TPA)-DBC]$^+$ has a distorted octahedral geometry with approximate C_s symmetry. The tripodal ligand coordinates to the iron with N_{amine}–Fe–$N_{pyridine}$ angles of less than 90° due to the five-membered chelates rings. The Fe–N(amine) at 2.221 (3) Å is comparable to those found for NTA and BPG complexes, 2.224 (3) and 2.218 (2) Å, respectively. The average value (2.124 Å) of the Fe–N(pyridine) trans to each other is also comparable to those found for [Fe(BPG)DBC][12] and $[Fe(TPA)Cl_2]^+$ [19] complexes, 2.144 and 2.126 Å, respectively. What distinguishes the TPA complex from the other two is the strength of the iron–catecholate interaction as indicated by the dramatic shortening of the Fe–O1A bond. For the NTA and BPG complexes, the DBC ligand chelates asymmetrically with $r_{Fe-O(DBC)}$ values of 1.887 (2) and 1.979 (2) Å and 1.889 (3) and 1.989 (3) Å, respectively. For the TPA complex, the asymmetry is significantly less pronounced and $r_{Fe-O(DBC)}$ values are 1.898 (2) and 1.917 (3) Å. This might be a result of the Fe–N(pyridine) interaction trans to the Fe–O1A bond in the TPA complex replacing Fe–O(carboxylate) bonds in the corresponding NTA and BPG complexes. At any rate, the complete replacement of carboxylates on the tripodal ligand with pyridines now leaves the catecholate as the only anionic ligand on the complex to interact with the very Lewis acidic metal center. This situation should enhance the covalency of the metal–catecholate bond(s) and lower the barrier for ligand-to-metal charge transfer as indicated by the low energy of the catecholate LMCT bands. It should be emphasized, however, that the bond lengths found for the DBC ligand (r_{C-O} = 1.347 (4), 1.349 (4) Å; r_{C1-C2} = 1.418 (5) Å) remain typical values for those expected for a chelated catecholate ligand.[10,20] The semiquinone character that may develop as a result of ligand-to-metal charge transfer is not

(18) Cromer, D. T.; Waber, J. T. *International Tables for X-ray Crystallography*; The Kynoch Press: Birmingham, England, 1974; Vol. IV, Table 2.2A.

(19) Yan, S.; Leising, R. A.; Que, L., Jr., unpublished results.

(20) (a) Raymond, K. N.; Isied, S. S.; Brown, L. D.; Fronczek, F. R.; Nibert, J. H. *J. Am. Chem. Soc.* **1976**, *98*, 1767. (b) Pierpont, C. G.; Buchanan, R. M. *Coord. Chem. Rev.* **1981**, *38*, 44. (c) Buchanan, R. M.; Wison-Blumenberg, C.; Trapp, C.; Larsen, S. K.; Greene, D. L.; Pierpont, G. G. *Inorg. Chem.* **1986**, *25*, 3070.

Table III. Comparison of the Properties of the [Fe(L)DBC] Complexes

	NTA[a]	PDA[b]	BPG[b]	TPA
λ_{max} (nm)[c]	408, 622	444, 688	488, 764	568, 883
intradiol cleavage yield	84%	95%	97%	98%
k_{O_2} in DMF (10^{-2} M^{-1} s^{-1})[d]	3.7	4.3	18	1500
k_{O_2} in MeOH (10^{-2} M^{-1} s^{-1})[d]	1.0	5.0	43	1000
δ (5-*t*- and 3-*t*-Bu) (ppm)[e]	3.9, 1.4[f]	5.1, 1.6	6.4, 4.6	8.7, 5.2
δ (DBC 6- and 4-H) (ppm)[g]	19, 14	16, 9	8, −18	−5, −57
δ (py meta H) (ppm)[e]		97, 81	95, 86	92, 90
$r_{Fe-O(DBC)}$ (Å)	1.887 (3), 1.979 (3)	nd	1.889 (2), 1.989 (2)	1.898 (2), 1.917 (3)

[a] Reference 10. [b] Reference 12. [c] Obtained in CH_3CN. [d] $k_{O_2} = k_{obs}/[O_2]$. [e] Remeasured in CD_3CN. [f] Obtained in CD_3CN/DMSO mixed solvent due to its lack of solubility. [g] Obtained by ^2H NMR of DBC-,6-d_2 complexes in DMF.

sufficiently large to affect the DBC bonds significantly. Clearly, the TPA complex has a coordinated catecholate, not a semiquinone.

Reactivity and Kinetics. The [Fe(L)DBC] complexes all react with dioxygen to yield products due to the oxidative cleavage of the catechol ring. The TPA complex affords intradiol cleavage products in nearly quantitative yield, thus the most specific of the oxidative cleavage systems. This observation is consistent with the trend earlier noted that the yield of intradiol cleavage product increases as the Lewis acidity of the metal center increases.[12] The two products isolated from the reaction mixture are 3,5-di-*tert*-butyl-1-oxacyclohepta-3,5-diene-2,7-dione (60%) and 3,5-di-*tert*-butyl-5-(carboxymethyl)-2-furanone (38%) as shown below:

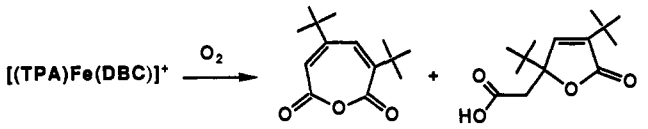

As earlier observed,[10,12] the anhydride is the product of oxidative cleavage. In this case, however, the Fe^{III}(TPA) center appears to promote hydrolysis of the anhydride to muconic acid and subsequent ring closure to form the furanone acid. This conversion results in the assembly of a (μ-oxo)diiron(III)–TPA complex with the furanone acid bridging the two metal centers, with UV–vis and NMR spectral properties corresponding to those of the $[Fe_2(TPA)_2O(C_{14}H_{21}O_4)]ClO_4)_3$ complex obtained by direct synthesis.

The TPA complex is the fastest reacting of all the [Fe(L)DBC] complexes studied. Kinetics studies of the reaction of the complex with 1 atm of O_2 in DMF under pseudo-first-order conditions show that the TPA complex reacts approximately three orders of magnitude faster than the corresponding NTA complex (Table III). The TPA result represents the most substantial jump in reaction rate relative to the next fastest complex in this series and completes the series reported by Cox and Que.[12] On the basis of the earlier arguments, both the high specificity and the fast kinetics can be associated with the high Lewis acidity of the ferric center in the TPA complex.

NMR Properties. The [Fe(L)DBC] complexes exhibit large NMR contact shifts, which provide some information regarding the electronic structure of the complexes.[12] In general, the NMR spectrum of the TPA complex is dominated by the pyridine meta protons, which appear as relatively sharp features at 92 and 90 ppm with T_1 values of 1.15 and 1.04 ms, respectively (Figure 2).[21] The pyridine ortho protons are broadened due to their proximity to the metal center and shifted further downfield at 196 ppm with a T_1 value of 0.13 ms. The pyridine para protons resonate in the diamagnetic region at 1.1 ppm, which can be obscured by other features. Additional peaks arise from the methylene protons, which appear as a broad band at 116 ppm with a T_1 value of 0.15 ms. The DBC 6-H and 4-H protons for the TPA complex exhibit shift at −0.2 and −55.4 ppm in CD_3CN, respectively. The assignments can be confirmed by the ^2H NMR spectrum of the selectively deuterated complex (Figure 2). The more downfield shifted resonance is the broader of the two protons and thus assigned to 6-H proton due to its proximity to the metal center. The DBC-5-*t*-Bu and 3-*t*-Bu proton resonances are found at 8.7 and 5.2 ppm with T_1 values of 5.68 and 0.83 ms, respectively.

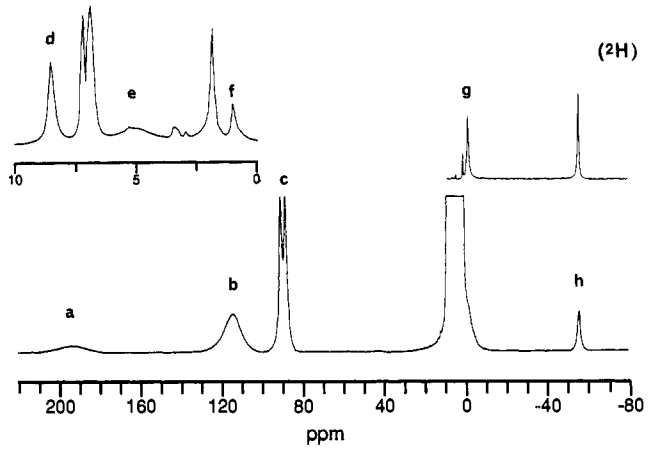

Figure 2. ^1H NMR spectrum of [Fe(TPA)DBC](BPh$_4$) in CD_3CN under argon with ambient conditions. The left inset is an expansion of the diamagnetic region of the main spectrum. The right inset is the ^2H NMR spectrum of [Fe(TPA)(DBC-*4,6-d*$_2$)])(BPh$_4$) in CH_3CN. The peaks refer to (a) py ortho H (196), (b) CH_2 (116), (c) py meta H (92, 90), (d) 5-*t*-Bu (8.7), (e) 3-*t*-Bu (5.2), (f) Py para H (1.1), (g) 6-H (−0.2), and (h) 4-H (−55.4 ppm) of TPA and DBC protons.[21] The two peaks at 7.3 and 7.0 ppm correspond to the protons of BPh_4.

Very strikingly, the catecholate shifts exhibit a remarkable dependence on the nature of the tetradentate ligands (Table III). The DBC 6-H and 4-H proton resonances go from being downfield shifted for the NTA and PDA complexes to being upfield shifted for the TPA complex. At the same time, the tripodal ligand shifts as monitored by the pyridine meta H's remain in the same downfield region for the entire series (Table III). The meta protons of pyridines bound to high-spin ferric centers such as $[Fe(TPA)Cl_2]^+$ are found at ~100 ppm, while those bound to high-spin ferrous centers such as $[Fe(TPA)Cl_2]$ are observed at ~55 ppm.[19] On the basis of these comparisons, all the pyridine meta H shifts in the [Fe(L)DBC] series are indicative of high-spin Fe(III), in agreement with the structural and UV–vis data. We attribute the large variation in the DBC shifts to an increased semiquinone character due to the enhanced covalency of the metal–catecholate interaction as the series progresses from NTA to TPA complex. This semiquinone character is too small to be manifested in the structural data. It also does not affect the pyridine isotropic shifts significantly because the isotropic shifts due to high-spin ferric and ferrous centers are comparable in magnitude. The semiquinone character is manifested in the DBC shifts because of the large differences in unpaired spin density expected for a catecholate coordinated to a paramagnetic center versus a seminquinone. A coordinated catecholate would gain unpaired spin density only via spin delocalization from the paramagnetic center, while a semiquinone is itself a paramagnetic center. The shift patterns for the various DBC protons are consistent with an increasing semquinone character from the NTA

(21) All peak assignments were based on the T_1 values and integrations and by comparison with the spectrum of the $[Fe(TPA)Cl_2]ClO_4$ complex.

to the TPA complex. EPR studies and MO calculations[22] on semiquinones have demonstrated substantial unpaired spin density at C-4 and C-5 and significantly smaller density at C-3 and C-6. Thus, the 5-*tert*-butyl exhibits a larger downfield shift relative to the 3-*tert*-butyl group, and the 4-H proton is significantly more upfield shifted than the 6-H proton. In the TPA complex, these effects are even more pronounced when compared to the other complexes. The greater semiquinone character in the TPA complex correlates well with its high reactivity toward O_2. These trends provide substantial support for the substrate activation mechanism we have proposed for the oxidative cleavage of catechols,[10] in which O_2 attack on the coordinated catecholate is facilitated by the enhanced radical character of the substrate (Scheme I). A peroxide complex is proposed to form subsequent to O_2 binding and then decomposes to the muconic anhydride. The recently reported crystal structure of the O_2 adduct of an Ir(III)-catecholate complex shows just such a peroxide moiety coordinated in a tridentate manner to the Ir center,[23] a result that lends further credence to the mechanism shown in Scheme I.

Acknowledgment. This research was supported by the National Institutes of Health Grants (GM-33162). We are grateful to Professor J. D. Britton for his expertise in the X-ray diffraction experiments.

Supplementary Material Available: Tables of atomic coordinates, thermal parameters, intermolecular distances, bond lengths, and bond angles for $[Fe^{III}(TPA)DBC]BPh_4$ (20 pages). Ordering information is given on any current masthead page.

(22) (a) Kahn, O.; Prins, R.; Reedijk, J.; Thompson, J. S. *Inorg. Chem.* **1987**, *26*, 3557. (b) Yamabe, S.; Minato, T.; Kimura, M. *J. Phys. Chem.* **1981**, *85*, 3510. (c) Trapp, C.; Tyson, C. A.; Giacometti, G. *J. Am. Chem. Soc.* **1968**, *90*, 1394.

(23) Barbaro, P.; Bianchini, C.; Mealli, C.; Meli, A. *J. Am. Chem. Soc.* **1991**, *113*, 3181.

Generation and Characterization of Dimolybdenum Thiyl Radicals

Ana C. Lizano, Martha G. Munchhof, Elaine K. Haub, and Mark E. Noble*

Contribution from the Department of Chemistry, University of Louisville, Louisville, Kentucky 40292. *Received May 15, 1991*

Abstract: Compounds of the type $[Mo_2(NC_6H_4CH_3)_2(S_2P(OC_2H_5)_2)_2S(O_2CCH_3)(SSR)]$, which contain RSS^- as Mo_2SSR units, and compounds of the type $[Mo_2(NC_6H_4R)_2(S_2P(OC_2H_5)_2)_2S_2(O_2CR')]_2$, which contain Mo_2SSMo_2 units, undergo photohomolysis with visible or ultraviolet light. Dimolybdothiyl radicals, $Mo_2S^\bullet$, are produced in all cases; these have been trapped and observed by EPR spectroscopy. Solvent reactions have shown that the radicals H abstract from tetrahydrofuran but not from chloroform nor from toluene. The radicals polymerize styrene and effect the cis-trans isomerization of 2-butene. A tetrasulfide derivative containing the $Mo_2SSSSMo_2$ unit also photolyzes to give polysulfides $Mo_2SSS_xSSMo_2$.

Introduction

While for some time there has been a great interest in syntheses and reactions of discrete metallosulfur complexes, there has also been within that general area a specific focus on sulfur-centered reactivity as opposed to, or in addition to, metal-centered reactivity. A wide variety of metallosulfur complexes have displayed sulfur-centered reactivity; among these, several systems have been particularly well developed, such as those of cyclopentadienylmetal and carbonyliron complexes.[1-4] Much of the interest in these systems has derived from the pivotal roles of metallosulfur systems in a variety of catalytic applications, and for which the question can therefore be posed as to whether the sulfur can interact with substrate in the catalytic mechanism.[1,2] Another interest lies in the similarity to organic sulfur chemistry which has been noted in many of the reactions. In such cases, sulfur ligands such as SH^-, S^{2-}, or S_2^{2-}, acting as terminal MS or bridge $M_2(\mu\text{-}S)$ units, showed parallel to thiol, thiolate and disulfide chemistry.[3-7] Noteworthy is that the bridge sulfur functionality is dicoordinate to metal and is therefore structurally similar to organic sulfides, R_2S, although in many cases its chemistry is distinctly thiolate in behavior.

Relative to organosulfur, one parallel in metallosulfur chemistry which has been less developed is sulfur-centered radical chemistry of a thiyl nature. This should not be too unexpected, however, since the metal itself within such a complex might accommodate the radical electron, thereby diminishing thiyl behavior.

One system which has displayed metallothiyl radical chemistry involves sulfidomolybdenum dimers of the type $[Mo_2(NAr)_2(S_2P(OEt)_2)_2(\mu\text{-}S)_2(\mu\text{-}O_2CR')]^\bullet$, **1** (for abbreviations, see note[8]), in which bridge sulfurs are the reactive species. The di-

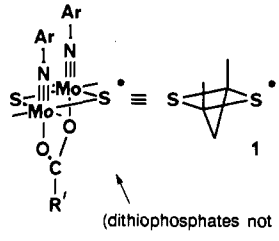

molybdothiyl complexes are not isolable per se but are instead generated in situ by photohomolysis of dimolybdenum(V) bisdimer disulfides $[Mo_2(NAr)_2(S_2P(OEt)_2)_2S_2(O_2CR')]_2$, **2**, or RSS-bridged dimers $[Mo_2(NAr)_2(S_2P(OEt)_2)_2S(O_2CR')(SSR)]$, **3** (eq 1). A number of reactions have been characterized for **1** in which

(1) Rakowski DuBois, M. *Chem. Rev.* **1989**, *89*, 1.
(2) Wachter, J. *Angew. Chem., Int. Ed. Engl.* **1989**, *28*, 1613.
(3) Seyferth, D.; Womack, G. B.; Henderson, R. S.; Cowie, M.; Hames, B. W. *Organometallics* **1986**, *5*, 1568 and references therein.
(4) Cowie, M.; DeKock, R. L.; Wagenmaker, T. R.; Seyferth, D.; Henderson, R. S.; Gallagher, M. K. *Organometallics* **1989**, *8*, 119 and references therein.
(5) Noble, M. E. *Inorg. Chem.* **1986**, *25*, 3311.
(6) Lizano, A. C.; Noble, M. E. *Inorg. Chem.* **1988**, *27*, 747.
(7) El-Hinnawi, M. A.; Al-Ajlouni, A. M. *J. Organomet. Chem.* **1987**, *332*, 321.

(8) Abbreviations used in this paper: Me, methyl; Et, ethyl; Pr, *n*-propyl; Bz, benzyl; Ar, aryl; Ph, phenyl; To, *p*-tolyl; Xy, *m*-xylyl (3,5-dimethylphenyl); Cp, cyclopentadienyl.

0002-7863/91/1513-9204$02.50/0 © 1991 American Chemical Society